molecules

MDPI

Article

Comparative Study of Polymer-Grafted $BaTiO_3$ Nanoparticles Synthesized Using Normal ATRP as Well as ATRP and ARGET-ATRP with Sacrificial Initiator with a Focus on Controlling the Polymer Graft Density and Molecular Weight

Ikeoluwa E. Apata [1], Bhausaheb V. Tawade [1], Steven P. Cummings [1], Nihar Pradhan [2], Alamgir Karim [3] and Dharmaraj Raghavan [1,*]

[1] Department of Chemistry, Howard University, Washington, DC 20059, USA; apatabett@gmail.com (I.E.A.); bvtawade@gmail.com (B.V.T.); steven.cummings@howard.edu (S.P.C.)
[2] Department of Chemistry, Physics and Atmospheric Science, Jackson State University, Jackson, MS 39217, USA; nihar.r.pradhan@jsums.edu
[3] Department of Chemical and Biomolecular Engineering, University of Houston, Houston, TX 77204, USA; akarim3@central.uh.edu
* Correspondence: draghavan@howard.edu

Abstract: Structurally well-defined polymer-grafted nanoparticle hybrids are highly sought after for a variety of applications, such as antifouling, mechanical reinforcement, separations, and sensing. Herein, we report the synthesis of poly(methyl methacrylate) grafted- and poly(styrene) grafted-$BaTiO_3$ nanoparticles using activator regeneration via electron transfer (ARGET ATRP) with a sacrificial initiator, atom transfer radical polymerization (normal ATRP), and ATRP with sacrificial initiator, to understand the role of the polymerization procedure in influencing the structure of nanoparticle hybrids. Irrespective of the polymerization procedure adopted for the synthesis of nanoparticle hybrids, we noticed PS grafted on the nanoparticles showed moderation in molecular weight and graft density (ranging from 30,400 to 83,900 g/mol and 0.122 to 0.067 chain/nm^2) compared to PMMA-grafted nanoparticles (ranging from 44,620 to 230,000 g/mol and 0.071 to 0.015 chain/nm^2). Reducing the polymerization time during ATRP has a significant impact on the molecular weight of polymer brushes grafted on the nanoparticles. PMMA-grafted nanoparticles synthesized using ATRP had lower graft density and considerably higher molecular weight compared to PS-grafted nanoparticles. However, the addition of a sacrificial initiator during ATRP resulted in moderation of the molecular weight and graft density of PMMA-grafted nanoparticles. The use of a sacrificial initiator along with ARGET offered the best control in achieving lower molecular weight and narrow dispersity for both PS (37,870 g/mol and PDI of 1.259) and PMMA (44,620 g/mol and PDI of 1.263) nanoparticle hybrid systems.

Keywords: PS-g-$BaTiO_3$ nanoparticles; PMMA-g-$BaTiO_3$ nanoparticles; ATRP; sacrificial initiator; ARGET

Citation: Apata, I.E.; Tawade, B.V.; Cummings, S.P.; Pradhan, N.; Karim, A.; Raghavan, D. Comparative Study of Polymer-Grafted $BaTiO_3$ Nanoparticles Synthesized Using Normal ATRP as Well as ATRP and ARGET-ATRP with Sacrificial Initiator with a Focus on Controlling the Polymer Graft Density and Molecular Weight. *Molecules* **2023**, *28*, 4444. https://doi.org/10.3390/molecules28114444

Academic Editor: Bhanu P. S. Chauhan

Received: 9 May 2023
Revised: 24 May 2023
Accepted: 26 May 2023
Published: 30 May 2023

1. Introduction

Polymer nanocomposites have been the focus of considerable research over the past several decades due to their ability to produce materials with a wide range of advanced properties [1–4]. $BaTiO_3$ nanoparticles are of particular interest among dielectric materials due to their superior dielectric permittivity, piezoelectric and ferroelectric properties, flexibility in adjusting their shape, and widespread use in energy storage, electronics, and device applications [5,6]. As a result, numerous methodologies for preparing $BaTiO_3$-based nanocomposites have been devised in order to increase the compatibility of the nanoparticles with the polymer matrix, the spatial dispersion of the nanoparticles in the matrix, and address the permittivity contrast between polymer and nanoparticles [7]. An

essential building block in formulating single-component or multicomponent polymer nanocomposites is the use of polymer-grafted nanoparticles hybrids [8–11]. Two main approaches have been used to synthesize polymer-grafted nanoparticle hybrids. The "*grafting to*" approach involves the attachment of end-functionalized polymer chains on the surface of nanoparticles via esterification, silylation, or click reactions, such as thiol-ene or alkyne-azide cycloaddition, to surface-activated nanoparticles [8]. An advantage of the "grafting to" approach is a monodisperse polymer on a nanoparticle surface can be achieved, allowing it to serve as an excellent model system. However, the bulkiness of long preformed polymer chains and steric hindrance limits the extent of grafting on the nanoparticle surface. More recently, new methods claim higher grafting densities can be achieved, even with the "grafting to" method [12,13].

The "*grafting-from*", also called surface-initiated control radical polymerization (*SI-CRP*), approach is based on growing polymer chains directly from the surface of nanoparticles functionalized with suitable initiator/CTA functionalities. The advantage of the "grafting from" method is the potential to achieve high grafting densities due to the ease of attaching a high number of monomers on the nanoparticle surface. However, the "grafting from" approach can be challenging because of the complex workup procedure, as well as particle aggregation. Many of these challenges have been addressed through the pioneering work of Matyjaszewski, [14] Mueller, [15] Benicewicz, [16] Takahara, [17] Hawker, [18], and coworkers. For example, good control over molecular weight distribution (MWD) in ATRP needs a certain deactivator concentration together with fast initiation to achieve uniform chain growth [19,20]. Typically, in conventional ATRP, a sufficiently high Cu catalyst concentration is needed to reach high monomer conversion [20–22]. However, the presence of a high amount of transition metal complexes may complicate polymer-grafted nanoparticle purification [22,23]. Therefore, minimal Cu(I) catalyst concentrations in ATRP are desirable but the trade-off is the broadening of MWD in grafted chains [24].

ARGET ATRP, indeed, addresses the purification of polymer-grafted nanoparticles, a problem arising due to the use of excessive copper catalysts during ATRP, by employing a lower copper concentration. The addition of sannous octoate ($Sn(Oct)_2$) as a reducing agent allows for continuous regeneration of Cu(I) (ATRP activator) from Cu(II) (ATRP deactivator), thereby lowering the total copper concentration needed to perform ATRP [24]. By adopting this method, Matyjaszewski et al. [25] demonstrated the synthesis of polystyrene (PS) grafts on SiO_2 nanoparticles (15 nm), with a low polydispersity of Đ = 1.17, using only 10 parts-per-million concentrations of copper (II) catalyst/L in relation to monomer [25]. However, it must be noted that the amount of $Cu(II)Br_2$ catalyst needed for grafting a polymer onto a nanoparticle may ultimately depend on the amount, size, and type of nanoparticles, and the amount of solvent and monomer used. By adopting a similar procedure in this study, we kept the concentration ratio of initiator-modified nanoparticles to $CuBr_2$ at 2x:1 similar to that reported by Matyjaszewski et al. [25] for 200 ppm nanoparticles to 100 ppm of $Cu(II)Br_2$.

In addition to the use of a Cu(II) pre-catalyst along with a reducing agent to synthesize grafted nanoparticles with less broadened MWD, a sacrificial initiator has also been used in the reaction medium [25–28]. The sacrificial initiator serves two purposes: one is to increase control over polymerization on the surface and the second is simply for analysis. Diffusion-controlled deactivation was enhanced when a sacrificial initiator was added to the polymerization mixture, playing a similar role to the well-known Trommsdorff effect, which brings about an increase in the polymerization rate for free-radical polymerization at high conversions [25–28]

Although a significant amount of research has been conducted on the grafting of polymers on SiO_2 nanoparticles using normal ATRP as well as ARGET ATRP [8,25,29], there has been limited work conducted on the synthesis of polymer-grafted $BaTiO_3$ nanoparticles using normal ATRP and ARGET ATRP [25,30]. More importantly, the use of a sacrificial initiator to control polymerization on the surface of $BaTiO_3$ nanoparticles using ATRP as well as ARGET has not been well studied outside of a few literature reports [31–37].

Thus, the primary objective of this study was to compare the graft density, dispersity, and molecular weight of polymer-grafted $BaTiO_3$ nanoparticles synthesized using ATRP and ARGET-ATRP techniques, with and without a sacrificial initiator. Our grafting study was not only limited to reactive methyl methacrylate (MMA) monomer but also extended to less reactive styrene monomers in the synthesis of PMMA-g-$BaTiO_3$ and PS-g- $BaTiO_3$, respectively. These grafted nanoparticles are widely used in several applications and serve as useful models for experimental studies.

2. Results and Discussion

For the synthesis of core–shell-structured PMMA-g-$BaTiO_3$ and PS-g-$BaTiO_3$ nanoparticles using ATRP and ARGET ATRP methods, the commercially available $BaTiO_3$ nanoparticles were subjected to a series of reactions, such as hydroxylation, silanization, and initiator attachment, to prepare the nanoparticle surface for polymer chain growth (Schemes 1 and 2). Figure 1A shows the IR for the steps performed to obtain initiator-grafted $BaTiO_3$ nanoparticles. The successful modification of nanoparticles was established via the appearance of a broad –OH absorption stretching band around 3400–3600 cm^{-1} upon the hydroxylation of $BaTiO_3$ nanoparticles, an alkyl stretching band at 2929 cm^{-1} due to the aliphatic –C-H and at 1566 cm^{-1} due to the N-H stretch upon silylation of the $BaTiO_3$ nanoparticles with APTMS; a carbonyl stretching band at 1650 cm^{-1} due to –CONH- (amide) upon initiator functionalization of $BaTiO_3$ nanoparticles with BIB. These observations were further substantiated by performing TGA analysis of the modified nanoparticles to successfully demonstrate the surface activation, functionalization, and modification of the $BaTiO_3$ nanoparticles with OH, APTMS, and BIB functional groups, respectively. As expected a gradual increase in weight loss in the order of $BaTiO_3$ < $BaTiO_3$-OH < $BaTiO_3$-APTMS < $BaTiO_3$-BIB was observed in the thermogram, which is consistent with the molar mass of functionality attached to the nanoparticles [35]. With the increase in grafted organic component onto nanoparticles, a more substantial drop in char yield was noticed.

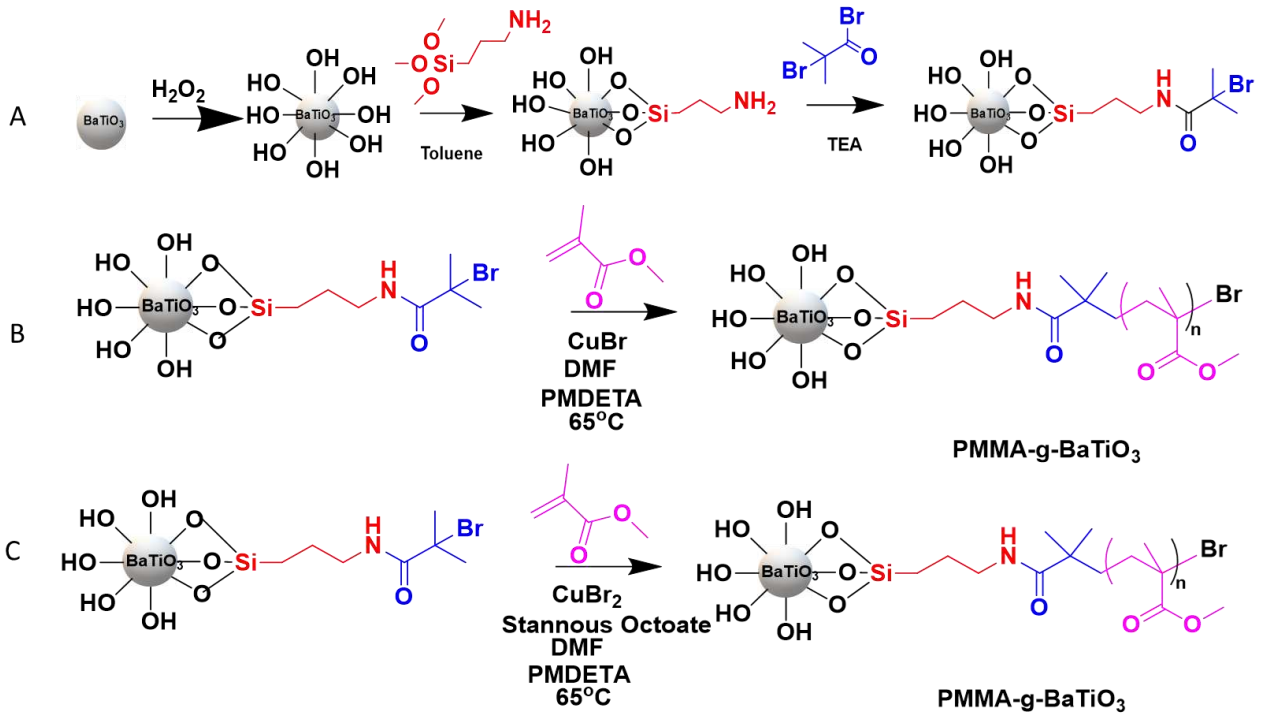

Scheme 1. (**A**) Modification, functionalization, and initiator grafted of $BaTiO_3$; (**B**) normal ATRP; (**C**) ARGET ATRP with sacrificial initiator synthetic route for PMMA-grafted $BaTiO_3$ nanoparticles.

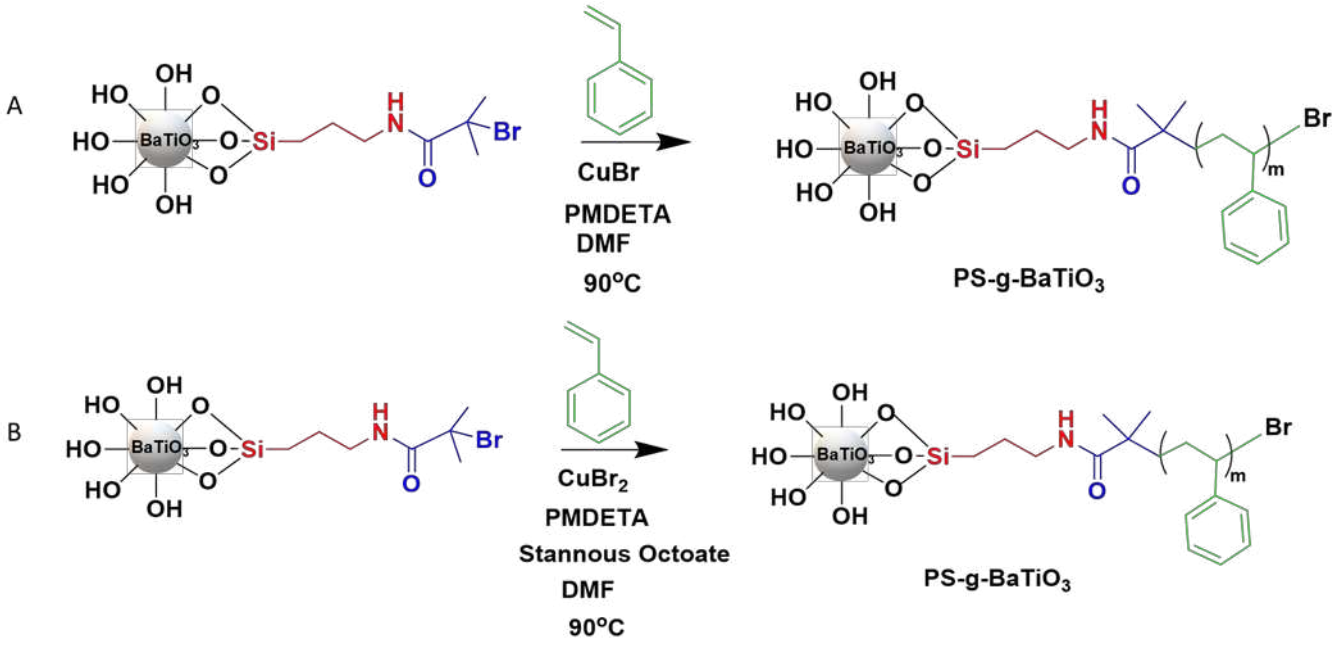

Scheme 2. (**A**) Normal ATRP; (**B**) ARGET ATRP with sacrificial initiators synthetic route for PS-grafted $BaTiO_3$ nanoparticles.

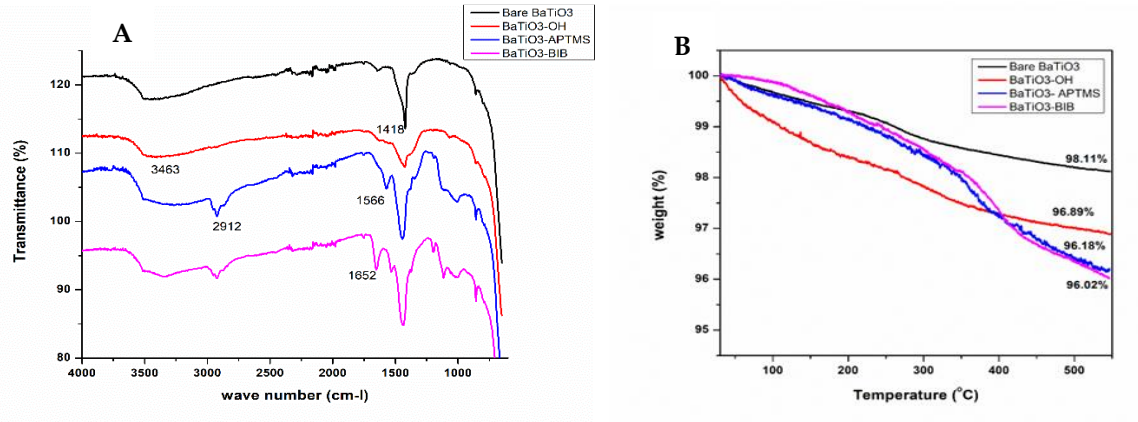

Figure 1. FT-IR spectra (**A**) and TGA thermogram (**B**) for bare ($BaTiO_3$), hydroxylated ($BaTiO_3$-OH) functionalized ($BaTiO_3$-APTMS), and initiator anchored ($BaTiO_3$-BIB) $BaTiO_3$ nanoparticles.

The grafting reaction of styrene and MMA on the surface $BaTiO_3$-BIB was carried out via ATRP in a "grafting from" approach by adopting the procedure previously reported by Xie et al. [35]. The FT-IR spectra (Figure 2A) of PMMA-g-$BaTiO_3$ show characteristic absorption bands at 2939 cm^{-1} (C–H groups), 1726 cm^{-1} (–C=O stretching), 1247 cm^{-1} (C-O stretching), and 1153 cm^{-1} (C-O-C stretching) [38]. Likewise, the FT-IR spectra (Figure 2B) for the PS-g-$BaTiO_3$ show a strong band at 3030 cm^{-1} (-CH aromatic stretching group), 1601 cm^{-1}, 1490 cm^{-1}, and 751 cm^{-1} (C=C aromatic group), consistent with the previously described observation for polystyrene grafted onto nanoparticles [39]. The intensity of the carbonyl peak of PMMA in PMMA-g-$BaTiO_3$ nanoparticles and the aromatic peak of PS in PS-g-$BaTiO_3$ nanoparticles varied with reaction time and procedure adopted. For example, a significant difference in the intensity of the FT-IR peaks (Figure 2A,B) of 24 h ATRP and the 12 h ARGET with a sacrificial initiator of PS and PMMA-grafted $BaTiO_3$ nanoparticles was noticed. More details about the influence of reaction time and condition on the characteristic of the polymer grafted on the nanoparticles will be discussed later.

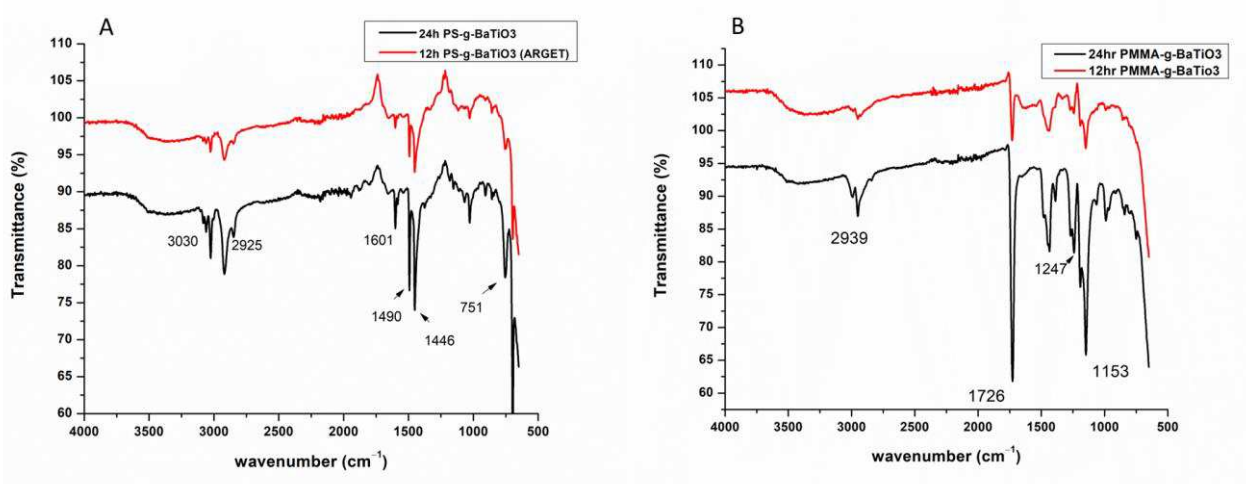

Figure 2. FT-IR spectra of (**A**) PS and (**B**) PMMA-grafted $BaTiO_3$ nanoparticles when the reaction was conducted for 12 h and 24 h.

To validate the successful grafting of the polymer on the surface of the nanoparticles, PS- and PMMA-grafted $BaTiO_3$ nanoparticles were subjected to a cleavage experiment. The cleaved polymer was characterized via ^{1}H-NMR and GPC analysis. The ^{1}H-NMR spectrum of the cleaved polymer from PS-g-$BaTiO_3$ nanoparticles (Figure 3) shows all the characteristic proton peaks for polystyrene. The aromatic protons (**c**, δ 6.56–7.31 ppm, =C−H), methylene (**b**, 0.82–1.24 ppm, −C−H), and the methine peak (**a**, 1.55–2.16, C−H) were observed in the NMR spectrum. Similarly, the ^{1}H-NMR spectrum for cleaved PMMA from PMMA-grafted $BaTiO_3$ shows methoxy methylene and methyl peaks, confirming the successful grafting of the PMMA on the polymer-grafted $BaTiO_3$ nanoparticle. The NMR spectrum for PMMA-g-$BaTiO_3$ was reported in our previous paper [7].

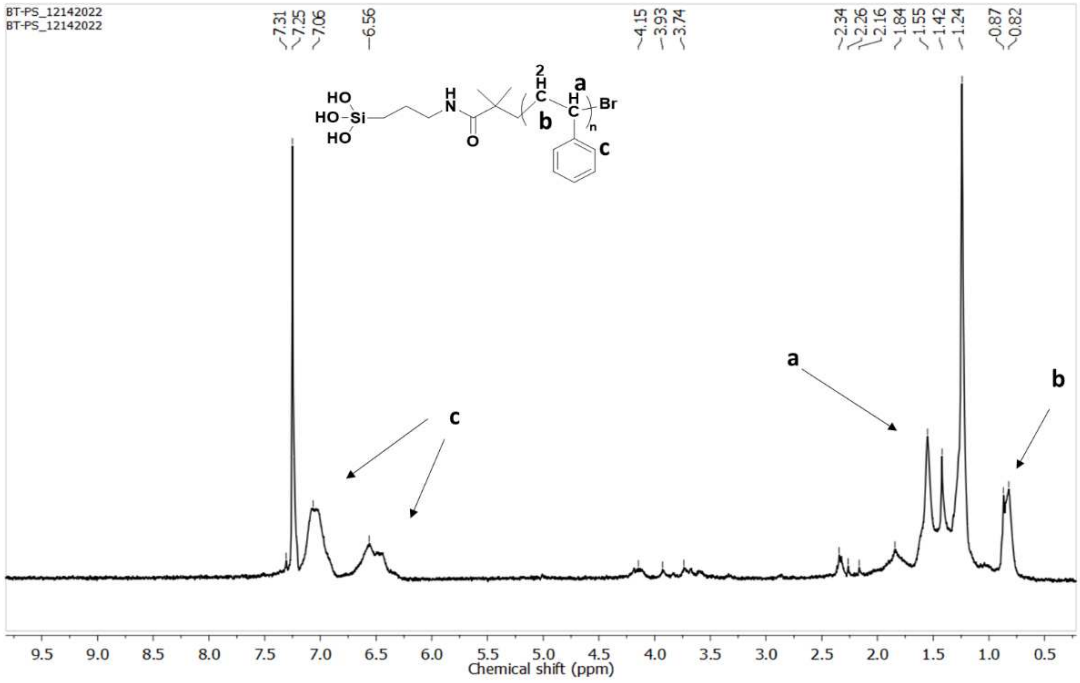

Figure 3. The ^{1}H-NMR spectrum for cleaved polystyrene from PS-grafted $BaTiO_3$ (PS-g-$BaTiO_3$ ATRP (24 h) nanoparticles. "**a**" in figure represents the methine proton, "**b**" is methylene proton peak, "**c**" is the aromatic proton peak.

Generally, a sacrificial initiator is added to the polymerization mixture and the supernatant is separated from the nanoparticles and precipitated to obtain free polymer chains that are grown in solution, as analyzed using GPC [40]. The major drawbacks to using this approach are that it neglects possible surface confinement and diffusion of the reactive components to and from the propagating radical ends and can result in different molecular weights and dispersity of surface-bound polymer chains compared to a free polymer in solution [41]. In this study, accurate molecular weight and dispersity of the grafted polymer were obtained by cleaving the polymer directly from the nanoparticle. A comparison the molecular weight and dispersity of the free polymer in solution was also determined to validate the aforementioned observation. For example, we observed that the molecular weight and dispersity of the free polymer chains (12 h ATRP with a sacrificial initiator was 16,990 g/mol and 1.213) were lower than that of the polymer cleaved (12 h ATRP with a sacrificial initiator was 30,400 g/mol and 1.522) from the surface of the nanoparticle. Consequently, in our subsequent studies, we determined the molecular weight of the cleaved polymer from the nanoparticles instead of analyzing the molecular weight of the polymer from solution.

Additionally, we performed transmission electron microscopy (TEM) measurements of the PS- and PMMA-grafted $BaTiO_3$ nanoparticles to observe the morphology and the dispersion of the homopolymer-grafted nanoparticles. Figure 4 shows representative TEM images of the polymer-grafted $BaTiO_3$ nanoparticles. The TEM image shows that the nanoparticles are nearly spherical or elliptical or cubic shaped. As expected, the TEM micrograph provides direct visual and clear evidence of two different regions in the polymer-grafted nanoparticles. We notice that the corona of nanoparticles has a different contrast and lighter texture (corresponding to less electron density polymeric material) than the center. It can be observed that the nanoparticles are homogeneously encapsulated by a layer of polymer, and the polymer-grafted nanoparticles are well dispersed. This shows that the grafting-from approach used in this study is indeed successful. As shown in Figure 5, we observed the polymer shell thickness to vary depending on the time and procedure used for the synthesis of polymer-grafted nanoparticles. The shell thickness of the 24 h PMMA-g-$BaTiO_3$ and PS-g-$BaTiO_3$ (Figure 5A,B) is approximately 17 nm and 10 nm, respectively, which is consistent with the higher molecular weight obtained for the 24 h PMMA-g-$BaTiO_3$, as compared to PS-g-$BaTiO_3$. Similar results were observed for the 12 h ARGET ATRP reaction with a sacrificial initiator. The shell thickness of PS-g-$BaTiO_3$ and PMMA-g-$BaTiO_3$ (Figure 5C,D) was approximately 7 nm and 5 nm, respectively. This observation is consistent with the lower molecular weight and lower char yield obtained for PS-g-$BaTiO_3$ and PMMA-g-$BaTiO_3$ nanoparticles after 12 h polymerization. These results further establish that the polymer was successfully grafted onto the surface of the BIB-modified $BaTiO_3$ nanoparticles via the various procedures adopted.

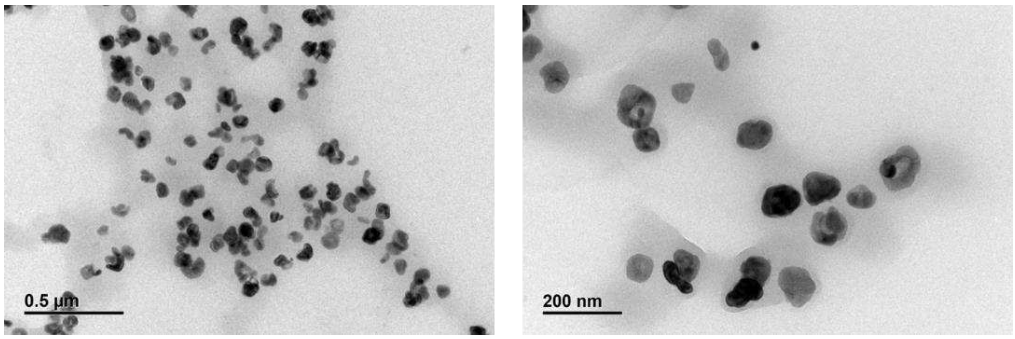

Figure 4. Representative TEM images showing the homogenous dispersion of the polymer-grafted nanoparticles (PS-g-$BaTiO_3$ Normal ATRP (24 h).

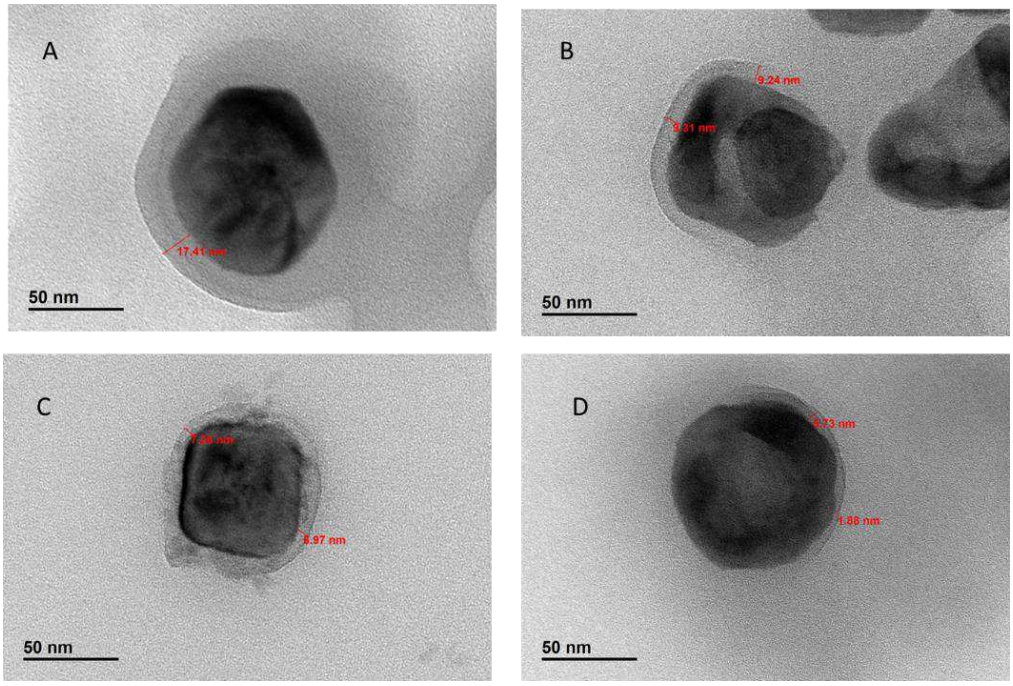

Figure 5. TEM image of (**A**) 24 h PMMA-g-$BaTiO_3$, (**B**) 24 h PS-g-$BaTiO_3$, (**C**) 12 h PMMA-g-$BaTiO_3$, and (**D**) 12 h PS-g-$BaTiO_3$.

PXRD analysis was carried out to determine what, if any, effects grafting had on the nanoparticle. Figure 6 presents the normalized XRD patterns of commercial $BaTiO_3$ and polymer-grafted $BaTiO_3$ nanoparticles. The PXRD patterns of the purchased and polymer-grafted nanoparticles exhibited characteristic crystallographic peaks at 22.2°, 31.5°, 38.9°, 45.2°, 50.9°, 56.2°, 65.9°, 70.4°, 74.9°, 79.2°, 83.5°, and 87.7°, as described in the figure. Using Bragg's law, the Miller indices were determined to be (100), (110), (111), (200), (210), (211), (220), (300), (310), (311), (222), and (320) for a face-centered cubic structure, in agreement with previously assigned literature values [42]. Grafting the polymer resulted in peak shifts not in excess of 0.2°, suggesting no significant changes to the topography of the nanoparticles. Sherrer's equation was applied to peaks at 31.5°, 56.2°, and 92.0° to determine the approximate sizes of the diffraction planes (FWHM was determined using the Rigaku SmartLab Studio II software suite). The relative standard deviation ranged between 3.5 and 5.8% from the commercial and polymer-grafted nanoparticles, confirming no significant influence of the pre-functionalization with initiators or the polymerization process on the crystallinity of the nanoparticle. One significant change from commercial $BaTiO_3$ for the polymer-grafted nanoparticles is the appearance of a broad peak with a 2θ max ranging between 11.6 and 12.1°. This peak is presumed to be due to the presence of the less-ordered polymer on the surface of the nanoparticle.

Effect of Reaction Times on ATRP-Synthesized Polymer-Grafted Nanoparticles

We evaluated the composition of PS- and PMMA-grafted $BaTiO_3$ nanoparticles when the synthesis was performed with the same feed ratio of the monomer to $BaTiO_3$-BIB nanoparticles while the ATRP reaction was conducted for 12 h and 24 h. The FT-IR spectra confirmed the observation of characteristic PS and PMMA peaks on the surface of the $BaTiO_3$ nanoparticle. Char residue from TGA was used to determine the amount of polymer grafted on the nanoparticles. Table 1 summarizes the characteristics of polymer-grafted nanoparticles synthesized using various methods. The char yield (which is primarily a measure of the inorganic $BaTiO_3$) for PS-grafted nanoparticles ranged from 72% to 85%, while the PMMA-grafted nanoparticle char yield ranged from 68.8% to 89%. For both systems, the char yield was found to increase significantly as the polymerization time was

reduced from 24 h to 12 h. Using the mass of the residual nanoparticles at 500 °C as a reference, a quantitative analysis of TGA data indicates that the amount of grafted polymer is proportionate to the molecular weight of the grafted polymer. Furthermore, the narrow dispersity obtained for all the grafted nanoparticles (PS- and PMMA-grafted nanoparticles) suggests that the ATRP is an effective controlled polymerization procedure [43].

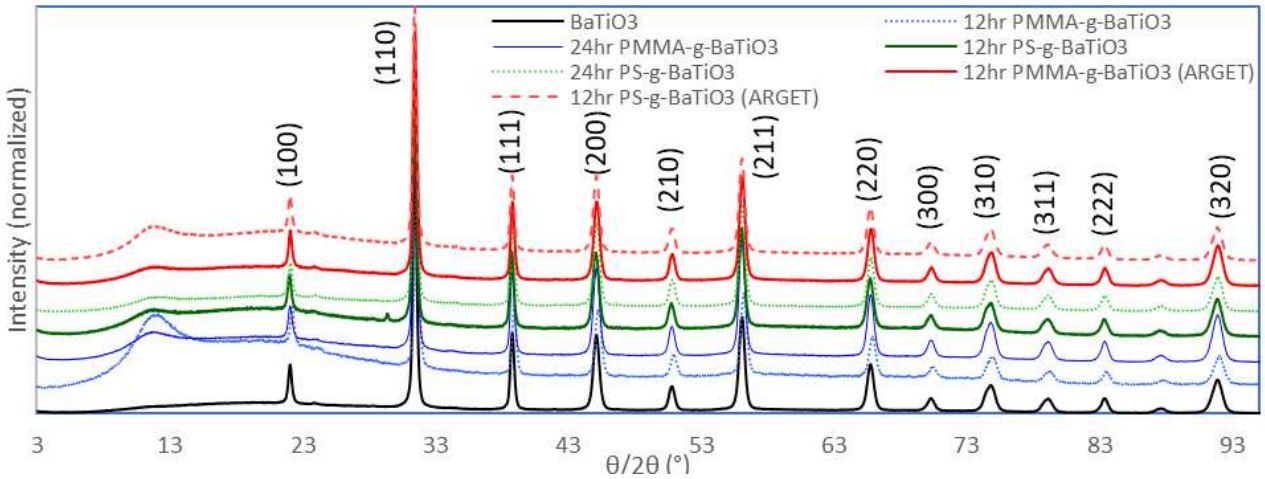

Figure 6. Normalized XRD patterns of commercial $BaTiO_3$ (black), PMMA-grafted $BaTiO_3$ (blue, 12 h—solid; 24 h—dashed); PS-grafted $BaTiO_3$ (green, 12 h—solid; 24 h—dashed) and PMMA with initiator (solid red); and PS-grafted $BaTiO_3$ with initiator (dashed red); 2θ was collected from 3° to 95° at 20 °C.

Table 1. Summary of the characterization of PS- and PMMA-grafted $BaTiO_3$ nanoparticle.

Samples (Polymerization Time)	TGA Char Yield of PGNPs, (%)	(Char Yield of BT NPs—Char Yield of PGNPs) (%)	Mn (g/mol) [a]	Mw (g/mol) [a]	Dispersity [a]	Graft Density (chain/nm^2)	Degree of Polymerization (DP)
PS-g-$BaTiO_3$ ATRP (24 h)	72	23.3	52,200	83.900	1.609	0.120	502
PS-g-$BaTiO_3$ ATRP (12 h)	85	10.6	20,600	31,100	1.514	0.122	198
PS-g-$BaTiO_3$ ATRP (EBIB) (12 h)	88.8	7.2	20,020	30,400	1.522	0.081	192
PS-g-$BaTiO_3$ ARGET (EBIB) (12 h)	88.4	7.4	30,090	37,870	1.259	0.067	289
PMMA-g-$BaTiO_3$ ATRP (24 h)	68.8	20.2	152,800	230,000	1.505	0.039	1528
PMMA-g-$BaTiO_3$ ATRP (12 h)	89	5.0	73,800	115,800	1.568	0.015	738
PMMA-g-$BaTiO_3$ ATRP (EBIB) (12 h)	85.6	10.4	29,390	52,080	1.775	0.071	294
PMMA-g-$BaTiO_3$ ARGET (EBIB) (12 h)	88.2	7.6	35,320	44,620	1.263	0.059	353

[a] Molecular weights measured for cleaved PMMA are not absolute molecular weights as GPC measurements were performed using PS calibration standards.

Although the weight loss of PMMA and PS grafted on the nanoparticles is similar based on TGA measurements, a significant difference in the average molecular weight of the two polymers was observed. Figure 7 shows a representative GPC chromatogram of 24 h and 12 h PS and PMMA polymer cleaved from polymer-grafted $BaTiO_3$ nanoparticles. PMMA has an average molecular weight of 115,800 g/mol and 230,000 g/mol for 12 h and 24 h reaction times, respectively (Table 1). On the other hand, the average molecular weight of PS was 31,100 g/mol and 83,900 g/mol for 12 h and 24 h reactions, respectively. The

molecular weight and char residue data were substituted in Equation (1) and used for calculating graft density. The graft density for PS was found to be 0.12 chains/nm^2, which was higher than that for PMMA 0.039 and 0.015 chains/nm^2 for identical polymerization times.

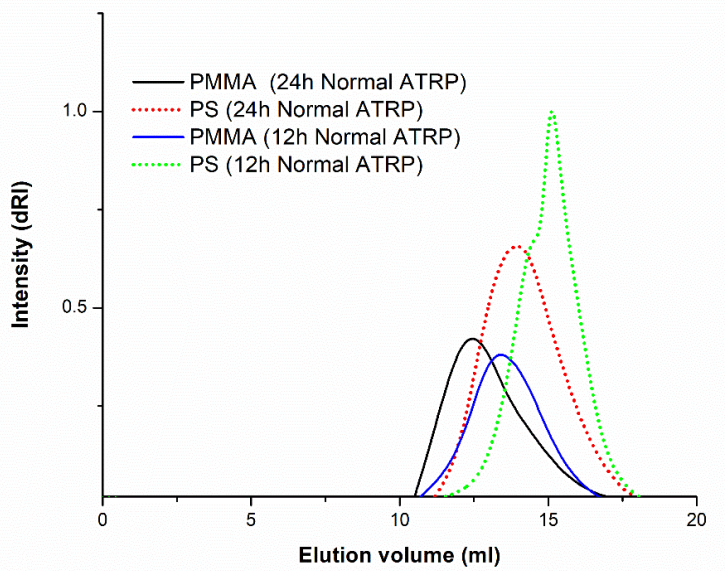

Figure 7. Representative GPC chromatogram of 24 h and 12 h PS and PMMA polymer cleaved from polymer-grafted $BaTiO_3$ nanoparticles.

Not all of the immobilized initiators can propagate with monomers to become polymer chains. For those that do, several factors influence the graft density of the polymer on the surface of the nanoparticles, such as the initiator bound on the surface, catalyst concentration, monomer structure (reactivity and stability of the intermediate radical species), solvent, catalyst-to-deactivator ratio used for polymerization, temperature, and time [44]. As reported earlier, the same amounts of initiator-grafted $BaTiO_3$ nanoparticles, catalyst, and solvent were used in the synthesis of PS- and PMMA-g-$BaTiO_3$ nanoparticles. The high graft density of PS compared to PMMA could be attributed to the polymerization condition. Polymerization of styrene on the nanoparticles was carried out at a higher temperature, which could also alleviate the monomer solubility and, hence, higher graft density. Liu et al. [45] used molecular dynamics simulations to investigate the effect of initiator density and polymerization rate on grafting density. For an ideal living surface-initiated polymerization system, they observed that a faster polymerization rate yields a lower grafting density [45]. Therefore, the lower graft density of PMMA-g-$BaTiO_3$ may be due to the higher rate of polymerization of the MMA monomer on $BaTiO_3$ compared to the styrene monomer. It is worth noting that this trend is observed for all the reaction procedures adopted in this study. The dispersity of PS-g-$BaTiO_3$ and PMMA-g-$BaTiO_3$ is (1.609 and 1.514) and (1.504 and 1.568) for the 12 h and 24 h polymerization times, respectively This shows that, even though the reaction time has a major effect on the rate of monomer conversion, which directly influences the molecular weight of the polymer grafted on the nanoparticles, the polydispersity was largely unaffected.

In l ATRP, molecular weight is controlled through the persistent radical effect, which suppresses termination reaction. Initially, a few percent of radical coupling is used to build up a concentration of deactivator, i.e., copper(II) species, which, in sufficient concentrations, will deactivate intermediate radicals faster than the rate at which the radicals can react in termination events [46]. However, chain termination is not completely eliminated during the course of polymerization. Figure 8 summarizes the four possible termination modes that could take place in graft polymerization from the surfaces of discrete particles and in the presence of free chains in solution. There could be termination between free chains in solution, between a free chain and a surface-bound chain, between chains on the

same particle surface, and between chains on different particle surfaces. Because some components can diffuse freely in the former two modes, the rates of termination involving free chains (in solution and to the surface) should be faster than those involving only surface-bound chains (intraparticle and interparticle) [30].

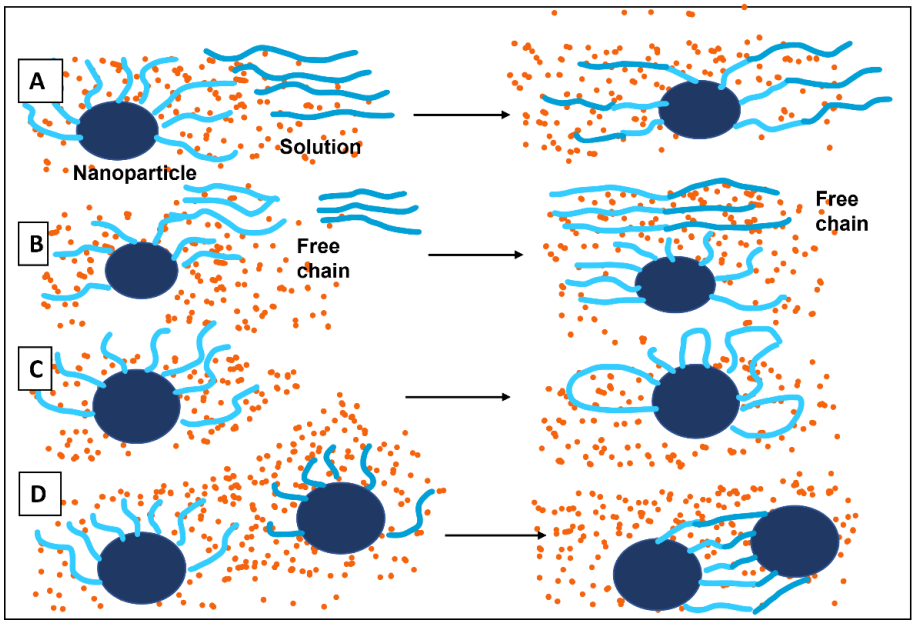

Figure 8. Possible termination modes that could take place in graft polymerization from the surfaces of discrete particles and in the presence of free chains in solution (the dots represent the solution): (**A**) between a free chain and a surface-bound chain, (**B**) between free chains in solution, (**C**) between chains on the same particle surface, (**D**) between chains on different particle surfaces.

Styrene can undergo thermal self-initiation at high temperatures. Because the styrene ATRP polymerization reaction is carried out at a temperature where thermal polymerization is significant (90 °C), some free polystyrene chains could be forming in the solution. This allows termination to occur predominately in solution, though presumably some fraction occurs in the surface-bound polymers. Thus, the surface-bound PS can grow relatively unhindered, and the radical concentration remains constant [30].

On the other hand, MMA does not undergo thermal self-initiation. Because of this, there are little to no free chains in solution during the MMA ATRP. Therefore, most chain termination occurs intraparticle or interparticle. Intra- and interparticle termination could result in the formation of a cross-linked structure over long polymerization. This could result in significantly high molar masses, as observed for PMMA-g-$BaTiO_3$ for the 24 h and 12 h polymerization time. Previous observations indicated that we could incorporate some molecular weight control in MMA ATRP by introducing minimal free chains into the solution during the polymerization process.

Two approaches were pursued to introduce free chains in the solution, i.e., ARGET with a sacrificial initiator, as well as ATRP with a sacrificial initiator. Ethyl 2-bromo-2-methylpropionate was used as the sacrificial initiator for the polymerization of styrene and the MMA monomer. This would allow for the growth of some free chains in the solution during the polymerization reaction. The polymerization reactions were conducted for 12 h because 12 h ATRP gave a moderately high molecular weight and better PDI for both PS and PMMA. As presented in Table 1, the TGA residual weight of 12 h ATRP with a sacrificial initiator for PS-g-$BaTiO_3$ decreased to 7.2% compared to 10.6% for the 12 h ATRP without sacrificial initiator. Additionally, a drop in the graft density from 0.12 chain/nm^2 to 0.081 chain/nm^2 occurred. The drop in the polymer grafting density can be due to the steric hindrance presented by the slightly higher molecular weight in the case of ATRP with a sacrificial initiator.

In the case of PMMA-g-$BaTiO_3$ nanoparticles, we observed a more than 50% decrease in the Mw upon the addition of a sacrificial initiator from 115,800 g/mol for normal ATRP to 52,080 g/mol. The grafting density of PMMA-g-$BaTiO_3$ nanoparticles increases (0.015 chain/nm^2 to 0.071 chain/nm^2) upon the addition of a sacrificial initiator, which suggests that many shorter chains are grafted on the surface of the nanoparticle upon the addition of the sacrificial initiator, as compared to the longer chains we observed in the normal ATRP of PMMA. For both normal ATRP and ATRP with a sacrificial initiator, we observed that the PDI was in a range of 1.5 to 1.7, which shows some good control of the dispersity using this method. However, better control of the polydispersity was obtained using ARGET with a sacrificial initiator, as discussed below.

For the ARGET ATRP with a sacrificial initiator, the Mw of PS-grafted chains increased from 30,000 g/mol to 37,000 g/mol, while the dispersity decreased from 1.5 to 1.259 compared to ATRP with a sacrificial initiator. Similar results were observed for PMMA-g-$BaTiO_3$ nanoparticles. For PMMA, the Mw slightly decreased from 52,080 g/mol to 44,620 g/mol, with a drastic drop in the PDI from 1.7 to 1.263 while performing ARGET ATRP with a sacrificial initiator compared to ATRP with a sacrificial initiator. The higher values of Mw indicate that longer PS and PMMA chains are grafted during the ARGET ATRP reaction, and the drop in the dispersity shows good control of the polymerization using ARGET with a sacrificial initiator. It is worth noting that the graft density of both PS- and PMMA-grafted $BaTiO_3$ also decreases in ARGET ATRP with a sacrificial initiator compared to ATRP with a sacrificial initiator. For example, the grafting density decreased from 0.081 chain/nm^2 to 0.067 chain/nm^2 and from 0.071 chains/nm^2 to 0.059 chains/nm^2 for PS- and PMMA-grafted $BaTiO_3$, respectively, indicating that ARGET ATRP favored the grafting of longer polymer chains with lower grafting densities compared with the ATRP method. The low graft densities can be attributed to the fact that surface initiation of $BaTiO_3$-BIB in ARGET ATRP is much lower than in ATRP, which is primarily a result of the use of a lower amount (ppm level) of catalyst [47].

3. Materials and Methods

$BaTiO_3$ nanoparticle (50 nm), 30% aq. H_2O_2 solution, (3-aminopropyl)trimethoxysilane (APTMS), α-bromoisobutyryl bromide (BIB), 98%, Sigma Aldrich, St. Louis, MO, USA, ethyl 2-bromo-2-methylpropionate (EBIB, 99%, Sigma Aldrich), anhydrous N,N′-dimethylformamide (DMF), N,N,N′,N′′,N′′-pentamethyldiethylenetriamine (PMDETA), stannous octoate, copper(II) bromide, copper(I) bromide, 40% hydrofluoric acid (HF), toluene, tetrahydrofuran (THF), an dichloromethane (DCM) were purchased from Sigma-Aldrich Chemical Company. Styrene and methylmethacrylate (MMA) were received from Thomas Scientific and distilled under a vacuum to remove the inhibitor before use, whereas all other reagents and solvents were used as received.

3.1. Synthesis of Core–Shell Nanoparticles

3.1.1. Surface-Initiated Atomic Transfer Radical Polymerization (ATRP)

For the synthesis of homopolymer core–shell nanoparticles using ATRP procedure, we slightly modified the *grafting-from* approach reported in the literature [35]. In our procedure, we used (3-aminopropyl) trimethoxysilane (APTMS) as the silane coupling agent instead of γ-aminopropyl triethoxysilane, as reported in [35], and the monomers were distilled under vacuum before use without washing with NaOH solution. Additionally, we performed sonication and stirred the mixture for 1 h prior to the reaction. Further, our polymer-grafted nanoparticles were dried under vacuum for 48 h in ambient conditions. Details about adopting the modified ATRP procedure for the synthesis of PMMA-g-$BaTiO_3$ have already been reported elsewhere [35,38].

Briefly, the nanoparticle was anchored with ATRP initiator by performing H_2O_2 hydroxylation, APTMS silylation followed by treatment with bromoisobutyryl bromide. The ATRP initiator-functionalized nanoparticle was then used for surface-initiated atom transfer polymerization (SI-ATRP) of monomer with various reaction times to obtain

polymer-grafted nanoparticles with varying molecular weights and graft densities. To graft polystyrene (PS) on the surface of 50 nm $BaTiO_3$ nanoparticle, initiator-anchored $BaTiO_3$-BIB and 12 mL DMF were placed in a Schlenk flask and interchangeably stirred and sonicated for 1 h. CuBr was added and the flask was sealed with a rubber plug. The oxygen in the flask was removed by backfilling with N_2 using a balloon. Styrene and (0.06 g, 72 µL) PMDETA were added via syringe to the reaction flask, and a freeze–thaw pump cycle was performed three times to degas the reaction mixture. The ratio of styrene:$BaTiO_3$-BIB:CuBr was kept as 13:1:0.5 [35]. This reaction mixture was then stirred at 90 °C for 24 h. After 24 h, the reaction was stopped by placing the flask in liquid nitrogen and exposing the contents to air. The obtained PS-grafted $BaTiO_3$ (PS-g-$BaTiO_3$) nanoparticles after polymerization and centrifugation were re-dispersed in THF and washed several times in acetone to remove the un-grafted polymer and unreacted monomer from the PS-g-$BaTiO_3$ nanoparticles. Both the polymer-grafted nanoparticles and the cleaved polymer from the grafted nanoparticles were subjected to extensive characterization. Additionally, we studied the effect of reaction time on synthesizing PS and PMMA-grafted $BaTiO_3$ nanoparticles of varying shell thickness and shell coverage by conducting polymerization for 12 and 24 h, while all other parameters were kept constant. We also adopted a minor modification to the procedure of ATRP technique for synthesis of PS-g-$BaTiO_3$ and PMMA-g-$BaTiO_3$, respectively, by adding ethyl 2-bromo-2-methylpropionate (EBIB) to the reaction mixture prior to degassing the system via freeze–pump–thaw cycles and purging with nitrogen gas so as to study the effect of sacrificial initiator on the structure of polymer grafts tethered to nanoparticles.

3.1.2. Activator Regeneration via Electron Transfer (ARGET) ATRP with Sacrificial Initiator for Synthesis of PS- and PMMA-Grafted $BaTiO_3$ Nanoparticles

Polymerization of PMMA-g-$BaTiO_3$ nanoparticles via ARGET ATRP was conducted by using a copper(II) complex that was reduced in situ using stannous octoate as the reducing agent. Initiator-anchored $BaTiO_3$-BIB and 12 mL DMF were placed in a Schlenk flask, and the flask was sealed with a rubber plug. The reaction mixture was sonicated for 45 min using an ultrasonicator, after which $CuBr_2$ and MMA monomer were added, and the mixture was stirred for 15 min. The ratio of monomer/initiator-modified nanoparticles/$CuBr_2$ was kept as 13:1.0:0.5 [25]. To the flask, 470µL PMDETA was added via syringe alongside 5 µL ethyl 2-bromo-2-methylpropionate. After the system was degassed through two freeze–pump–thaw cycles and purged with nitrogen gas, stannous octoate (72 µL) was added via syringe under N_2 atmosphere to trigger the polymerization prior to performing a third freeze–pump–thaw cycle. The Schlenk flask was then placed in an oil bath set at 65 °C for 12 h. The reaction was quenched by immersing it into liquid nitrogen and exposing the contents to air. The product was recovered via centrifugation at 10,000 rpm for 10 min. The recovered polymer-grafted $BaTiO_3$ nanoparticles were redispersed in acetone to remove un-grafted PMMA and unreacted monomer.

The synthesis of PS-g-$BaTiO_3$ nanoparticle was similar to that of PMMA-g-$BaTiO_3$ nanoparticle using ARGET ATRP method except that the polymerization was carried out at 90 °C for 12 h in an oil bath. The workup to recover PS-g-$BaTiO_3$ nanoparticles was identical to the procedure described earlier.

The washed and recovered grafted nanoparticles were dried under a vacuum for 48 h. The product was used for FT-IR, TGA, TEM, and PXRD characterization, in addition to cleavage experiments.

3.2. Characterization of Polymer-Grafted $BaTiO_3$ Nanoparticles

In order to characterize the grafted polymer on the surface of the nanoparticles, the polymer-grafted nanoparticles were subjected to a cleavage experiment using HF in THF. Details about cleaving the polymer from the grafted nanoparticles and recovery of PMMA or PS via precipitation in hexane can be found elsewhere [38]. The recovered cleaved PS and PMMA were characterized using nuclear magnetic resonance (NMR) and gel permeation chromatography (GPC) techniques.

Molecular weight measurements of cleaved polymers were performed using gel permeation chromatography (GPC) on Agilent Technologies 1260 Infinity. The samples obtained from the cleavage experiment were dissolved in THF and filtered using a 0.2 μm syringe filter. Polystyrene standards were used for calibration. THF was used as the eluent, and the cleaved polymer concentration was maintained at about 1 mg mL^{-1}.

^{1}H NMR spectra of cleaved homopolymer were recorded on Bruker AVANCE 400 MHz NMR spectrometer using chloroform-d as the solvent. Chemical shifts given in parts per million (δ ppm) were relative to tetramethylsilane (TMS) and referenced to residual $CDCl_3$ at 7.26 ppm.

Fourier-transform infrared spectroscopy (FT-IR) spectra of all the precursors used for polymer-grafted nanoparticles ($BaTiO_3$-OH, $BaTiO_3$-APTMS, and $BaTiO_3$-BIB) as well as the polymer-grafted nanoparticle were collected using a Perkin-Elmer ATR-FT-IR Spectrum 100 Series. A minimum of 16 scans were collected in a range of 4000 to 650 cm^{-1}, and triplicate measurements were performed to confirm the reproducibility of IR spectra.

Thermogravimetric analysis (TGA) of all the precursors and polymer-grafted nanoparticles was conducted using a TGA/DTA 320 Seiko instrument under a nitrogen atmosphere (flow rate of 100 mL min^{-1}). The thermogram was generated by placing nearly 10 mg of samples in a pan and heating it from 30 °C to 600 °C at a heating rate of 10 °C per minute. The char yields were used to calculate the amount of polymer grafted on the nanoparticle as well as the graft density of the core–shell structure. The graft density was calculated using Equation (1) below.

$$\sigma_{TGA} = \frac{\frac{wt\ \%_{shell}}{wt\ \%_{core}} \rho_{core} \frac{4}{3} \pi {r_{core}}^3 N_A}{M_w 4 \pi {r_{core}}^2} \quad (1)$$

where mass % of shell = difference in char yield of BT nanoparticle and that of PGNPs; mass % of core = Char yield of BT nanoparticle, N_A = Avogadro's number, ρ_{core} = 6.09 g/cm^3 which represent the density of bulk $BaTiO_3$, r_{core} = 50 nm, corresponding to the radius of $BaTiO_3$ assuming a spherical shape, and M_W = Mass average molecular mass of cleaved polymer chains.

Transmission electron microscopy (TEM) analysis was conducted to characterize the shell thickness and dispersion of the homopolymer-grafted nanoparticle in film-casting solvent. To prepare TEM samples, about 2 mg of the grafted nanoparticle samples was dispersed in 3 mL of DMF and sonicated for 1 h. The solution was further diluted using serial dilution. The diluted solution was cast on a 200-mesh carbon-coated copper grid (Electron Microscopy Science, Hatfield, PA, USA). The cast film was left overnight in air at room temperature to dry. The dried sample was preserved in a vacuum desiccator until further use. TEM micrographs of dried samples were collected with a JEM 2100 LaB6 TEM at Nanoscale Imaging, Spectroscopy, and Properties Facility at University of Maryland, College Park.

Powder X-ray diffractometry (XRD) was performed to determine what, if any, influence the polymerization process had on the crystal structure of $BaTiO_3$ nanoparticles. The wide-angle X-ray diffraction of the functionalized and polymer-grafted $BaTiO_3$ nanoparticles was collected using a Rigaku MiniFlex X-ray powder diffractometer (Cu Kα radiation λ = 1.5418 Å) from 3° to 90° at a scan rate of 0.0166 °/s (λ = 1.5418 Å) (40 kV, 15 mA), with a step size of 0.010° and a step time of 0.6 s.

4. Conclusions

In the present study, ARGET ATRP with a sacrificial initiator and normal ATRP with and without a sacrificial initiator were employed for the synthesis of PMMA/PS-grafted $BaTiO_3$ nanoparticles. PMMA/PS-grafted $BaTiO_3$ nanoparticles were characterized using FT-IR and ^{1}H-NMR to confirm their chemical structure, while TGA was used for estimation of the % of polymer grafted on the NP surface. The cleaved polymer samples were analyzed via GPC for the determination of molar masses and dispersity. TEM analysis confirmed the successful grafting of PMMA and PS on the surface of $BaTiO_3$ nanoparticles, with

shell thickness in a range of 5–17 nm. The effect of time on the molecular weight and dispersity was also investigated, and it revealed livingness of polymerization reactions, and molecular weights increased with polymerization time. The variation in the molecular weight and graft density with respect to polymerization conditions, monomer reactivity, monomer solubility in solvent, and time was explained, and plausible pathways for polymerization termination were provided. It was observed that a sacrificial initiator played an important role in controlling the dispersity and lowering the molecular weights, as compared to ATRP without a sacrificial initiator. Further, ARGET with a sacrificial initiator had better control of polymer grafts of both MMA and styrene on $BaTiO_3$ nanoparticles. The present results provide a la carte approaches to synthesize polymer-grafted $BaTiO_3$ nanoparticles with defined molecular weights and narrow dispersity. The ability to tune the structure of polymer-grafted nanoparticle hybrids, depending on the selection of the methodology, opens the door for material design, depending upon the intended application and the requirements.

Author Contributions: Conceptualization, I.E.A., D.R. and B.V.T.; methodology, I.E.A. and B.V.T.; formal analysis, I.E.A., B.V.T. and S.P.C.; investigation, I.E.A. and B.V.T.; writing—original draft preparation, I.E.A. and D.R.; writing—review and editing, I.E.A., D.R., B.V.T. and S.P.C.; supervision, D.R.; project administration, D.R.; funding acquisition, D.R., N.P. and A.K. All authors have read and agreed to the published version of the manuscript.

Funding: This research was funded by the National Science Foundation (NSF), grant numbers DMR-1901127 and DMR-2117502. Rigaku MiniFlex X-ray powder diffractometer used in this study was funded by the National Science Foundation (NSF), grant number DMR-2117502.

Institutional Review Board Statement: Not applicable.

Informed Consent Statement: Not applicable.

Data Availability Statement: Not applicable.

Acknowledgments: The authors acknowledge the financial support from NSF DMR-1901127-POL. The authors thank Stephen Boyes and Rhys Dickhudt from George Washington University, Washington DC, for access to GPC instrument. The authors would like to thank Jiancun Rao Advanced Imaging & Microscopy (AIM) Laboratory at University of Maryland, College Park, for help with TEM analysis.

Conflicts of Interest: The authors declare no conflict of interest.

References

1. Yan, J.; Bockstaller, M.R.; Matyjaszewski, K. Brush-modified materials: Control of molecular architecture, assembly behavior, properties and applications. *Prog. Polym. Sci.* **2020**, *100*, 101180. [CrossRef]
2. Shameem, M.M.; Sasikanth, S.M.; Annamalai, R.; Raman, R.G. A brief review on polymer nanocomposites and its applications. *Mater. Today Proc.* **2021**, *45*, 2536–2539. [CrossRef]
3. Singh, M.; Apata, I.; Samant, S.; Wu, W.; Tawade, B.; Pradhan, N.; Raghavan, D.; Karim, A. Nanoscale Strategies to Enhance the Energy Storage Capacity of Polymeric Dielectric Capacitors: Review of Recent Advances. *Polym. Rev.* **2021**, *62*, 211–260. [CrossRef]
4. Tawade, B.V.; Apata, I.E.; Singh, M.; Das, P.; Pradhan, N.; Al-Enizi, A.M.; Karim, A.; Raghavan, D. Recent developments in the synthesis of chemically modified nanomaterials for use in dielectric and electronics applications. *Nanotechnology* **2021**, *32*, 142004. [CrossRef]
5. Cai, Q.J.; Gan, Y.; Chan-Park, M.B.; Yang, H.B.; Lu, Z.S.; Li, C.M.; Guo, J.; Dong, Z.L. Solution-processable barium titanate and strontium titanate nanoparticle dielectrics for low-voltage organic thin-film transistors. *Chem. Mater.* **2009**, *21*, 3153–3161. [CrossRef]
6. Hong, K.; Lee, T.H.; Suh, J.M.; Yoon, S.-H.; Jang, H.W. Perspectives and challenges in multilayer ceramic capacitors for next generation electronics. *J. Mater. Chem. C* **2019**, *7*, 9782–9802. [CrossRef]
7. Tawade, B.V.; Singh, M.; Apata, I.E.; Veerasamy, J.; Pradhan, N.; Karim, A.; Douglas, J.F.; Raghavan, D. Polymer-Grafted Nanoparticles with Variable Grafting Densities for High Energy Density Polymeric Nanocomposite Dielectric Capacitors. *JACS Au* **2023**, *3*, 1365–1375. [CrossRef]
8. Tawade, B.V.; Apata, I.E.; Pradhan, N.; Karim, A.; Raghavan, D. Recent Advances in the Synthesis of Polymer-Grafted Low-K and High-K Nanoparticles for Dielectric and Electronic Applications. *Molecules* **2021**, *26*, 2942. [CrossRef]

9. Chancellor, A.J.; Seymour, B.T.; Zhao, B. Characterizing Polymer-Grafted Nanoparticles: From Basic Defining Parameters to Behavior in Solvents and Self-Assembled Structures. *Anal. Chem.* **2019**, *91*, 6391–6402. [CrossRef]
10. Ma, S.; Zhang, X.; Yu, B.; Zhou, F. Brushing up functional materials. *NPG Asia Mater.* **2019**, *11*, 24. [CrossRef]
11. Francis, R.; Joy, N.; Aparna, E.P.; Vijayan, R. Polymer grafted inorganic nanoparticles, preparation, properties, and applications: A review. *Polym. Rev.* **2014**, *54*, 268–347. [CrossRef]
12. Ehlert, S.; Taheri, S.M.; Pirner, D.; Drechsler, M.; Schmidt, H.W.; Förster, S. Polymer ligand exchange to control stabilization and compatibilization of nanocrystals. *ACS Nano* **2014**, *8*, 6114–6122. [CrossRef]
13. Shui, Y.; Su, Y.; Kuang, X.; Zhao, W.; Cai, Y.; Wang, D. Facile and controllable synthesis of hybrid silica nanoparticles densely grafted with poly(ethylene glycol). *Polym. Int.* **2017**, *66*, 1395–1401. [CrossRef]
14. Matyjaszewski, K.; Miller, P.J.; Shukla, N.; Immaraporn, B.; Gelman, A.; Luokala, B.B.; Siclovan, T.M.; Kickelbick, G.; Vallant, T.; Hoffmann, H.; et al. Polymers at Interfaces: Using Atom Transfer Radical Polymerization in the Controlled Growth of Homopolymers and Block Copolymers from Silicon Surfaces in the Absence of Untethered Sacrificial Initiator. *Macromolecules* **1999**, *32*, 8716–8724. [CrossRef]
15. Cheng, G.; Böker, A.; Zhang, M.; Krausch, G.; Müller, A.H.E. Amphiphilic Cylindrical Core−Shell Brushes via a "Grafting From" Process Using ATRP. *Macromolecules* **2001**, *34*, 6883–6888. [CrossRef]
16. Li, C.; Benicewicz, B.C. Synthesis of well-defined polymer brushes grafted onto silica nanoparticles via surface reversible addition-fragmentation chain transfer polymerization. *Macromolecules* **2005**, *38*, 5929–5936. [CrossRef]
17. Matsuno, R.; Yamamoto, K.; Otsuka, H.; Takahara, A. Polystyrene-Grafted Magnetite Nanoparticles Prepared through Surface-Initiated Nitroxyl-Mediated Radical Polymerization. *Chem. Mater.* **2003**, *15*, 3–5. [CrossRef]
18. Husseman, M.; Malmström, E.E.; McNamara, M.; Mate, M.; Mecerreyes, D.; Benoit, D.G.; Hedrick, J.L.; Mansky, P.; Huang, E.; Russell, T.P.; et al. Controlled Synthesis of Polymer Brushes by "Living" Free Radical Polymerization Techniques. *Macromolecules* **1999**, *32*, 1424–1431. [CrossRef]
19. Min, K.; Gao, H.; Matyjaszewski, K. Preparation of homopolymers and block copolymers in miniemulsion by ATRP using activators generated by electron transfer (AGET). *J. Am. Chem. Soc.* **2005**, *127*, 3825–3830. [CrossRef]
20. Krys, P.; Matyjaszewski, K. Kinetics of Atom Transfer Radical Polymerization. *Eur. Polym. J.* **2017**, *89*, 482–523. [CrossRef]
21. Tang, H.; Arulsamy, N.; Radosz, M.; Shen, Y.; Tsarevsky, N.V.; Braunecker, W.A.; Tang, W.; Matyjaszewski, K. Highly active copper-based catalyst for atom transfer radical polymerization. *J. Am. Chem. Soc.* **2006**, *128*, 16277–16285. [CrossRef] [PubMed]
22. Ribelli, T.G.; Lorandi, F.; Fantin, M.; Matyjaszewski, K. Atom Transfer Radical Polymerization: Billion Times More Active Catalysts and New Initiation Systems. *Macromol. Rapid Commun.* **2019**, *40*, 1800616. [CrossRef] [PubMed]
23. Tsubokawa, N. Surface grafting of polymers onto nanoparticles in a solvent-free dry-system and applications of polymer-grafted nanoparticles as novel functional hybrid materials. *Polym. J.* **2007**, *39*, 983–1000. [CrossRef]
24. Dworakowska, S.; Lorandi, F.; Gorczyński, A.; Matyjaszewski, K. Toward Green Atom Transfer Radical Polymerization: Current Status and Future Challenges. *Adv. Sci.* **2022**, *9*, 2106076. [CrossRef]
25. Wang, Z.; Yan, J.; Liu, T.; Wei, Q.; Li, S.; Olszewski, M.; Wu, J.; Sobieski, J.; Fantin, M.; Bockstaller, M.R.; et al. Control of Dispersity and Grafting Density of Particle Brushes by Variation of ATRP Catalyst Concentration. *ACS Macro Lett.* **2019**, *8*, 859–864. [CrossRef]
26. Benetti, E.M.; Kang, C.; Mandal, J.; Divandari, M.; Spencer, N.D. Modulation of Surface-Initiated ATRP by Confinement: Mechanism and Applications. *Macromolecules* **2017**, *50*, 5711–5718. [CrossRef]
27. Mohammad Rabea, A.; Zhu, S. Controlled radical polymerization at high conversion: Bulk ICAR ATRP of methyl methacrylate. *Ind. Eng. Chem. Res.* **2014**, *53*, 3472–3477. [CrossRef]
28. Zhu, S.; Tian, Y.; Hamielec, A.E.; Eaton, D.R. Radical trapping and termination in free-radical polymerization of mma. *Macromolecules* **1990**, *23*, 1144–1150. [CrossRef]
29. Wang, Z.; Lee, J.; Wang, Z.; Zhao, Y.; Yan, J.; Lin, Y.; Li, S.; Liu, T.; Olszewski, M.; Pietrasik, J.; et al. Tunable Assembly of Block Copolymer Tethered Particle Brushes by Surface-Initiated Atom Transfer Radical Polymerization. *ACS Macro Lett.* **2020**, *9*, 806–812. [CrossRef]
30. von Werne, T.; Patten, T.E. Atom transfer radical polymerization from nanoparticles: A tool for the preparation of well-defined hybrid nanostructures and for understanding the chemistry of controlled/"living" radical polymerizations from surfaces. *J. Am. Chem. Soc.* **2001**, *123*, 7497–7505. [CrossRef]
31. Paniagua, S.A.; Kim, Y.; Henry, K.; Kumar, R.; Perry, J.W.; Marder, S.R. Surface-initiated polymerization from barium titanate nanoparticles for hybrid dielectric capacitors. *ACS Appl. Mater. Interfaces* **2014**, *6*, 3477–3482. [CrossRef]
32. Zhang, X.; Zhao, S.; Wang, F.; Ma, Y.; Wang, L.; Chen, D.; Zhao, C.; Yang, W. Improving dielectric properties of $BaTiO_3$/poly(vinylidene fluoride) composites by employing core-shell structured $BaTiO_3$@Poly(methylmethacrylate) and $BaTiO_3$@Poly(trifluoroethyl methacrylate) nanoparticles. *Appl. Surf. Sci.* **2017**, *403*, 71–79. [CrossRef]
33. Zhang, X.; Chen, H.; Ma, Y.; Zhao, C.; Yang, W. Preparation and dielectric properties of core–shell structural composites of poly(1H,1H,2H,2H-perfluorooctyl methacrylate)@BaTiO3 nanoparticles. *Appl. Surf. Sci.* **2013**, *277*, 121–127. [CrossRef]
34. You, N.; Zhang, C.; Liang, Y.; Zhang, Q.; Fu, P.; Liu, M.; Zhao, Q.; Cui, Z.; Pang, X. Facile Fabrication of Size-Tunable Core/Shell Ferroelectric/Polymeric Nanoparticles with Tailorable Dielectric Properties via Organocatalyzed Atom Transfer Radical Polymerization Driven by Visible Light. *Sci. Rep.* **2019**, *9*, 1869. [CrossRef] [PubMed]

35. Xie, L.; Huang, X.; Wu, C.; Jiang, P. Core-shell structured poly(methyl methacrylate)/BaTiO3 nanocomposites prepared by in situ atom transfer radical polymerization: A route to high dielectric constant materials with the inherent low loss of the base polymer. *J. Mater. Chem.* **2011**, *21*, 5897–5906. [CrossRef]
36. Wang, J.; Guan, F.; Cui, L.; Pan, J.; Wang, Q.; Zhu, L. Achieving high electric energy storage in a polymer nanocomposite at low filling ratios using a highly polarizable phthalocyanine interphase. *J. Polym. Sci. Part B Polym. Phys.* **2014**, *52*, 1669–1680. [CrossRef]
37. Xie, L.; Huang, X.; Huang, Y.; Yang, K.; Jiang, P. Core@Double-shell structured $BaTiO_3$-polymer nanocomposites with high dielectric constant and low dielectric loss for energy Storage Application. *J. Phys. Chem. C* **2013**, *117*, 22525–22537. [CrossRef]
38. Samant, S.; Hailu, S.; Singh, M.; Pradhan, N.; Yager, K.; Al-Enizi, A.M.; Raghavan, D.; Karim, A. Alignment frustration in block copolymer films with block copolymer grafted TiO2 nanoparticles under soft-shear cold zone annealing. *Polym. Adv. Technol.* **2021**, *32*, 2052–2060. [CrossRef]
39. Kim, K.; Park, M.S.; Na, Y.; Choi, J.; Jenekhe, S.A.; Kim, F.S. Preparation and application of polystyrene-grafted alumina core-shell nanoparticles for dielectric surface passivation in solution-processed polymer thin film transistors. *Org. Electron.* **2019**, *65*, 305–310. [CrossRef]
40. Askar, S.; Li, L.; Torkelson, J.M. Polystyrene-Grafted Silica Nanoparticles: Investigating the Molecular Weight Dependence of Glass Transition and Fragility Behavior. *Macromolecules* **2017**, *50*, 1589–1598. [CrossRef]
41. Turgman-Cohen, S.; Genzer, J. Computer simulation of controlled radical polymerization: Effect of chain confinement due to initiator grafting density and solvent quality in "grafting from" method. *Macromolecules* **2010**, *43*, 9567–9577. [CrossRef]
42. Pasuk, I.; Neațu, F.; Neațu, Ș.; Florea, M.; Istrate, C.M.; Pintilie, I.; Pintilie, L. Structural details of batio3 nano-powders deduced from the anisotropic xrd peak broadening. *Nanomaterials* **2021**, *11*, 1121. [CrossRef] [PubMed]
43. Li, D.; Sheng, X.; Zhao, B. Environmentally responsive "hairy" nanoparticles: Mixed homopolymer brushes on silica nanoparticles synthesized by living radical polymerization techniques. *J. Am. Chem. Soc.* **2005**, *127*, 6248–6256. [CrossRef] [PubMed]
44. Mastan, E.; Xi, L.; Zhu, S. Factors Affecting Grafting Density in Surface-Initiated ATRP: A Simulation Study. *Macromol. Theory Simulations* **2016**, *25*, 220–228. [CrossRef]
45. Liu, H.; Li, M.; Lu, Z.Y.; Zhang, Z.G.; Sun, C.C. Influence of Surface-Initiated Polymerization Rate and Initiator Density on the Properties of Polymer Brushes. *Macromolecules* **2009**, *42*, 2863–2872. [CrossRef]
46. Matyjaszewski, K.; Patten, T.E.; Xia, J. Controlled/'living' radical polymerization. Kinetics of the homogeneous atom transfer radical polymerization of styrene. *J. Am. Chem. Soc.* **1997**, *119*, 674–680. [CrossRef]
47. Zhang, Z.; Wang, X.; Tam, K.C.; Sèbe, G. A comparative study on grafting polymers from cellulose nanocrystals via surface-initiated atom transfer radical polymerization (ATRP) and activator re-generated by electron transfer ATRP. *Carbohydr. Polym.* **2019**, *205*, 322–329. [CrossRef]